Eur. Phys. J. A (2024) 60:157
https://doi.org/10.1140/epja/s10050-024-01369-5

THE EUROPEAN PHYSICAL JOURNAL A

Regular Article - Experimental Physics

Study of quasi-projectile properties at Fermi energies in ^{48}Ca projectile systems

FAZIA Collaboration

S. Upadhyaya[1,2,a], K. Mazurek[2], T. Kozik[1], D. Gruyer[3], G. Casini[4], S. Piantelli[4], L. Baldesi[4,5], S. Barlini[4,5], B. Borderie[6], R. Bougault[3], A. Camaiani[4,5], C. Ciampi[7], M. Cicerchia[8,9], M. Ciemała[2], D. Dell'Aquila[10,11], J. A. Dueñas[12], Q. Fable[13], J. D. Frankland[7], F. Gramegna[14], M. Henri[15], B. Hong[16,17], A. Kordyasz[18], M. J. Kweon[19], N. Le Neindre[3], I. Lombardo[20,21], O. Lopez[3], T. Marchi[14], S. H. Nam[16,17], J. Park[16,17], M. Pârlog[3,22], G. Pasquali[4,5], S. Valdré[4], G. Verde[13,20], E. Vient[3], M. Vigilante[11]

[1] Marian Smoluchowski Institute of Physics, Jagiellonian University, 30-348 Kraków, Poland
[2] Institute of Nuclear Physics Polish Academy of Sciences (IFJ-PAN), 31-342 Kraków, Poland
[3] LPC Caen UMR6534, ENSICAEN, CNRS/IN2P3, Université de Caen Normandie, 14000 Caen, France
[4] INFN-Sezione di Firenze, 50019 Sesto Fiorentino, Italy
[5] Dipartimento di Fisica e Astronomia, Università di Firenze, 50019 Sesto Fiorentino, Italy
[6] IJCLab, CNRS/IN2P3, Université Paris-Saclay, 91405 Orsay, France
[7] Grand Accélérateur National d'Ions Lourds (GANIL), CEA/DRF-CNRS/IN2P3, Boulevard Henri Becquerel, 14076 Caen, France
[8] Dipartimento di Fisica e Astronomia, University of Padova, Padua, Italy
[9] INFN-Sezione di Padova, 35121 Padua, Italy
[10] Dipartimento di Fisica "Ettore Pancini", University of Naples "Federico II", Naples, Italy
[11] INFN-Sezione di Napoli, Naples, Italy
[12] Departamento de Ingeniería Eléctrica y Centro de Estudios Avanzados en Física, Matemáticas y Computación, Universidad de Huelva, 21007 Huelva, Spain
[13] Laboratoire des 2 Infinis-Toulouse (L2IT-IN2P3), Université de Toulouse, CNRS, UPS, 31062 Toulouse Cedex 9, France
[14] INFN-Laboratori Nazionali di Legnaro, 35020 Legnaro, Italy
[15] CEA/INSTN/UECC, Les Vindits-143, Chemin de la Crespinière, 50130 Cherbourg-Octeville, France
[16] Center for Extreme Nuclear Matters (CENuM), Korea University, Seoul 02841, Republic of Korea
[17] Department of Physics, Korea University, Seoul 02841, Republic of Korea
[18] Heavy Ion Laboratory, University of Warsaw, 02-093 Warsaw, Poland
[19] Department of Physics, Inha University, Incheon 22212, Republic of Korea
[20] INFN-Sezione di Catania, 95123 Catania, Italy
[21] Dipartimento di Fisica e Astronomia, Università di Catania, Via S. Sofia 64, 95123 Catania, Italy
[22] National Institute for Physics and Nuclear Engineering, 077125 Bucharest-Măgurele, Romania

Received: 19 February 2024 / Accepted: 23 June 2024 / Published online: 26 July 2024

Communicated by Takashi Nakamura

Abstract A systematic analysis of the data obtained by the FAZIA collaboration during a recent experiment with a neutron rich projectile is presented. The main goal was to compare the experimental results with the HIPSE event generator simulations to investigate the influence of the neutron rich entrance channel on the quasi-projectile fragment properties. The full isotopic range of charged particles detected in this experiment was within the limit of the resolution of the FAZIA detector. A majority of quasi-projectile fragments were detected thanks to the forward angular acceptance of the experimental setup which was confirmed through the HIPSE calculations. Essentially, the lowering of N/Z of quasi-projectile fragments with the beam energy was found to be present since the initial phase of the reaction. Thus, pre-equilibrium neutron emissions might be a possible candidate to explain such an effect.

1 Introduction

Nuclear reactions in the intermediate energy range (20–100 MeV/u) have been of interest in studying various nuclear properties with respect to the beam energy, mass of the system and centrality of the collision. Excitation energies of hot

[a] e-mail: sahil.upadhyaya@ifj.edu.pl (corresponding author)

nuclei in these reactions can be close to or even higher than their total binding energies. The production of a large range of fragments is one of the main features of such reactions, as a consequence of the various processes that are responsible for fragment emission, spread over different time scales.

From an experimental point of view, the most important factor in studying such reactions is a high capability of identifying the charge (Z) and mass (A) of each emitted fragment. Among the many particle identification devices [1–6], the one designed and developed by the FAZIA collaboration [7] represents the state of the art for this kind of studies at Fermi energies. At present, the FAZIA detectors are able to identify the mass of fragments with charges up to $Z \sim 25$; for the present reactions (light systems at Fermi energies), this allows us to basically cover the entire phase-space region of quasi-projectile fragments. This was achieved mainly by using silicon detectors with high dopant homogeneity obtained with the n-TD process and specific crystallographic orientation. These Si detectors were used in reverse mounting so that the particles enter from the low-field side. The usage of dedicated pre-amplifiers, located as close as possible to the detector and extensive optimization of the digital treatment of the sampled pulse shapes of both charge and current signals. See Ref. [7] and references therein for details about the various optimisations done by the FAZIA collaboration to achieve excellent isotopic identification capabilities. The identification procedures are discussed in detail in Ref. [8] for $\Delta E - E$ method and in Ref. [9] for pulse-shape analysis (PSA).

With this excellent isotopic resolution of FAZIA, numerous experimental endeavors have been devoted to the investigation of isospin (neutron-to-proton ratio – N/Z) related physics (for example, see Refs. [10–16]). This was mainly realized by using projectile-target combinations with different N/Z compositions. The isospin degree of freedom and its influence on the reaction dynamics and on the subsequent decay processes has been widely studied by various groups (see Refs. [17–22] and references therein). The experimental observables associated with the isospin content of the reaction products can be used to extract information on the symmetry energy (E_{sym}) term of the nuclear equation of state ($nEoS$), via comparison with theoretical models, Refs. [17,18,20–40] and study isospin transport (differential flux of neutrons vs protons and nucleon density) in dissipative collisions at low energies, e.g. Refs. [41,42] and at Fermi energies, Refs. [19,27–31,34,43–49].

In this paper, we show a systematic analysis of data obtained in a recent FAZIA experiment by bombarding a neutron rich ^{48}Ca projectile at 25 MeV/u and 40 MeV/u on ^{12}C, ^{27}Al and ^{40}Ca targets. The experiment was based on an approach to study the effects of a neutron rich projectile on the properties of reaction products mainly for semi-peripheral/peripheral collisions. These collisions are basically binary dissipative events which lead to the production of two main primary fragments, a quasi-projectile (QP) and a quasi-target (QT). The experimental data are also compared with the simulations produced by the HIPSE (Heavy-Ion Phase Space Exploration) event generator [50,51].

The initial conditions of neutron richness can be diminished due to pre-equilibrium (fast) emissions from the projectile. These pre-equilibrium emissions were reported for neutrons and light particles within the Fermi energy range with the pre-equilibrium neutron multiplicity increasing with the beam energy [52]. For our reactions which are being induced by a neutron rich projectile, if there is an even slightly larger probability for fast neutron emission versus charged emissions (e.g. more free neutrons than protons), this will result in a net loss of neutron richness of the remaining system. Our goal here is to observe the effect of this diminished neutron richness in the first phases of the reaction on the QP fragment with the help of HIPSE. However, there is an important point to be mentioned that in the case of light ^{12}C target, the description based on the binary channel scenario weakens due to the strong size asymmetry of the entrance channel [10]. In this case, apart from very peripheral collisions, the reactions mostly form a single excited source (a kind of composite system) more than a real pair $QP - QT$. However, since we are interested in the events more ascribable to semi-peripheral reactions, the heavier fragment in the events is of our main concern, although we are aware that the association of this fragment as the QP is more valid for the reaction on ^{27}Al or ^{40}Ca than on ^{12}C. On the other hand, the data for ^{40}Ca target system is present only for 25 MeV/u beam energy and cannot be used to check beam energy dependence on fragment properties. With these "caveats" in mind, in the initial part of the paper, we decided to show the results for all systems for a clearer systematic and comparative analysis.

This article is organised in such a way that in Sect. 2, the details of the experimental setup along with a discussion on the obtained experimental data are given. The information about the HIPSE event generator and simulated data filtering is given in Sects. 3, and 4 discusses the conditions introduced according to the HIPSE predictions on the experimental data for QP fragment selection and shows further comparison between the experimental data and simulations. Summary and conclusion are given in the Sect. 5.

2 Experimental setup and data

The FAZIA-PRE experiment (discussed in Ref. [10]) was performed at the Laboratori Nazionali del Sud (LNS-INFN), Catania, Italy using 6 FAZIA blocks (Fig. 1) placed 1 m far from the target inside the LNS-Ciclope chamber. Therefore, a total of 96 (6 × 16) Si (300 μm)-Si (300/500 μm)-CsI (10 cm) telescopes were used. The overall angular coverage of

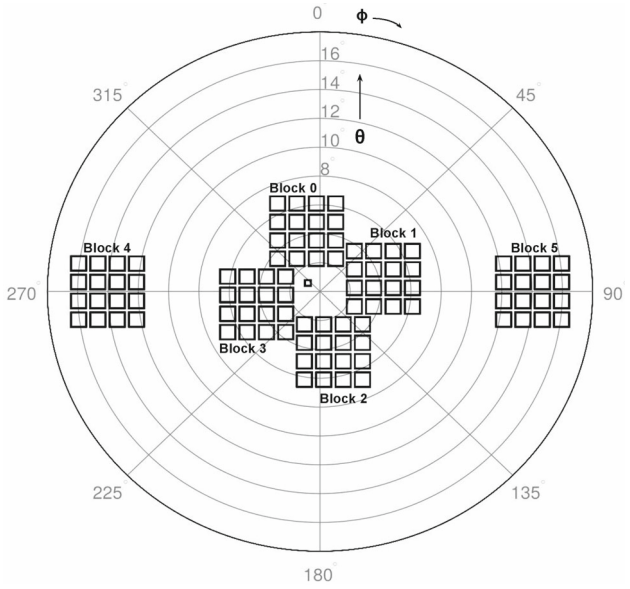

Fig. 1 Polar representation of the detector geometry of FAZIA-PRE experimental setup with the corresponding angular coverage. The four blocks in wall configuration cover ∼1.7–7.6° of θ. The remaining 2 blocks on the sides have a coverage of ∼11.5–16.7° of θ. Directions of used polar coordinates, θ and ϕ are marked

the detector setup was in the range θ ∼1.7–7.6° and ∼11.5–16.7° as shown in Fig. 1. The blocks were mounted in a way, such that, the central point of each cell (2x2 cm^2) points to the target (within 0.8°). The energy calibration methods for this experiment were performed as commonly done in other such FAZIA experiments (see Refs. [53,54]).

In this experiment, ^{48}Ca beams bombarded ^{12}C, ^{27}Al and ^{40}Ca targets at 25 MeV/u and, ^{12}C and ^{27}Al targets at 40 MeV/u. As said, the motivation for this choice of reaction systems is to study the fragment properties in the presence of a neutron rich entrance channel. The ^{48}Ca projectile is a n-rich nucleus with $N/Z = 1.4$. The targets ^{12}C and ^{40}Ca are symmetric ($N/Z = 1$) and ^{27}Al has one extra neutron making its $N/Z = 1.07$. The N/Z of the whole system ($N/Z_{\text{proj+tar}}$) ranges from 1.2 to 1.31. The values are shown in the Table 1 along with other experimental details like their corresponding target thicknesses (t), beam velocities (v_B), centre-of-mass velocities (v_{CM}), energies in centre-of-mass (E_{CM}), total isospin of the system ($N/Z_{\text{proj+tar}}$) and grazing angles in laboratory frame (θ_{gr}).

The forward angular acceptance of the experimental setup allows the QP fragments to be detected efficiently. The QT fragments cannot be detected because they are mainly spread at relatively large polar angles and cannot reach the detector at such forward angles. This fact can be well observed from the Fig. 2 which shows the charge Z and parallel velocity ($v_\parallel$) correlation in the laboratory frame for all the detected fragments. As expected, for all the five systems under consideration, the Z vs $v_\parallel$ correlation presents an intense region around the projectile Z (= 20) and the corresponding beam velocities ($v_\parallel = v_B$) marked by black dashed vertical lines. This intense region in the data corresponds to the QP fragments. The centre-of-mass velocity ($v_\parallel = v_{CM}$) is also marked for each system by red dashed vertical lines.

The characteristics of measured fragments can be better seen, though still in an inclusive way, by plotting the charge and mass distributions for all systems (see Fig. 3). We observe a peak around $Z \sim 20$ and $A \sim 40$, corresponding to the QP fragments measured in the most peripheral events, while some elastic scattering remaining for the low-energy beam reactions due to higher grazing angles (see Table 1). These peaks clearly stand out (a factor of about 10 more) from the rest of the distributions and give the bright yellow bin in the corresponding correlations in Fig. 2. In other words, from Figs. 2 and 3, one can remark that at 25 MeV/u, the more symmetric reactions are dominated by QP fragments (also very close to the projectile by about 10 times). The A and Z distributions for the more asymmetric case (^{12}C target) are broader, being associated to a more dispersed primary phase-space mixing various cases of fusion-like events. With

Table 1 FAZIA-PRE experimental details. $^{48}_{20}$Ca projectile on $^{12}_{6}$C, $^{27}_{13}$Al and $^{40}_{20}$Ca targets at 25 and 40 MeV/u beam energies (E_B) along with their corresponding target thicknesses (t), beam velocities (v_B), centre-of-mass velocities (v_{CM}), energies in centre-of-mass (E_{CM}), total isospin of the system ($N/Z_{\text{proj+tar}}$) and grazing angles in laboratory frame (θ_{gr})

Projectile	$^{48}_{20}$Ca				
E_B [MeV/u]	25	25	25	40	40
Target	$^{12}_{6}$C	$^{27}_{13}$Al	$^{40}_{20}$Ca	$^{12}_{6}$C	$^{27}_{13}$Al
t [μg/cm^2]	239	216	500	239	216
v_B [cm/ns]	6.8	6.8	6.8	8.5	8.5
v_{CM} [cm/ns]	5.5	4.4	3.8	7.0	5.5
E_{CM} [MeV/u]	4.0	5.7	6.2	6.4	9.2
$N/Z_{\text{proj+tar}}$	1.31	1.27	1.2	1.31	1.27
θ_{gr}	0.9°	1.8°	2.7°	0.5°	1.1°

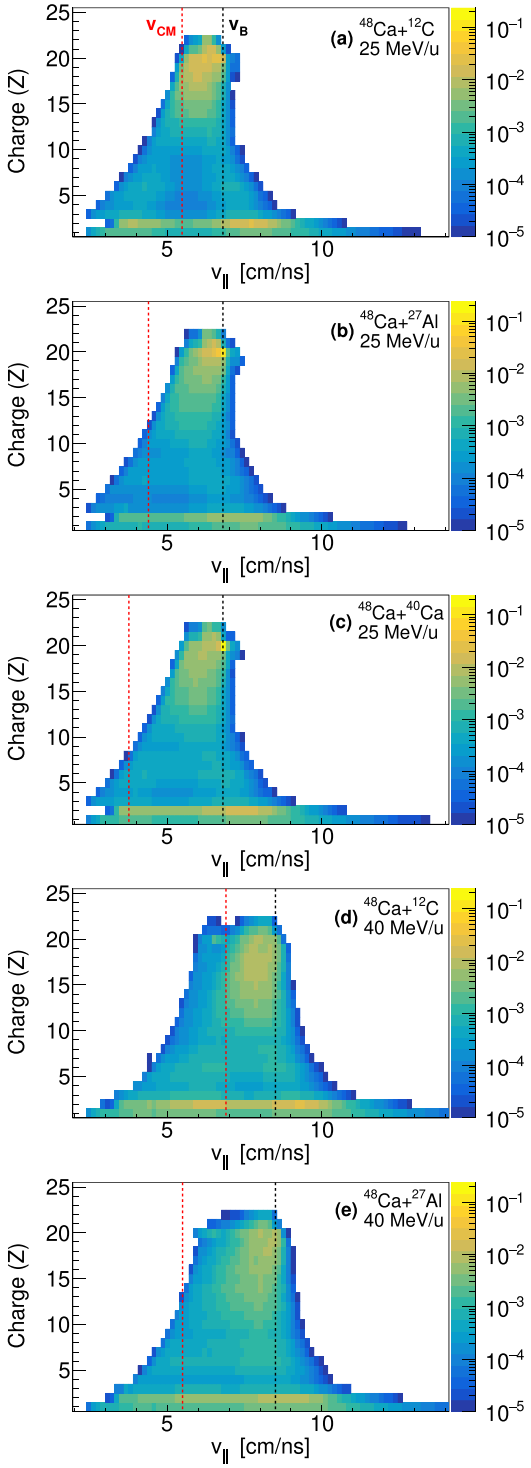

Fig. 2 Experimental data: fragment charge (Z) vs parallel velocity ($v_\parallel$) for all fragments detected in the FAZIA-PRE experiment. All systems are shown. Vertical red and black dashed lines show the corresponding centre-of-mass velocities (v_{CM}) and beam velocities (v_B), respectively

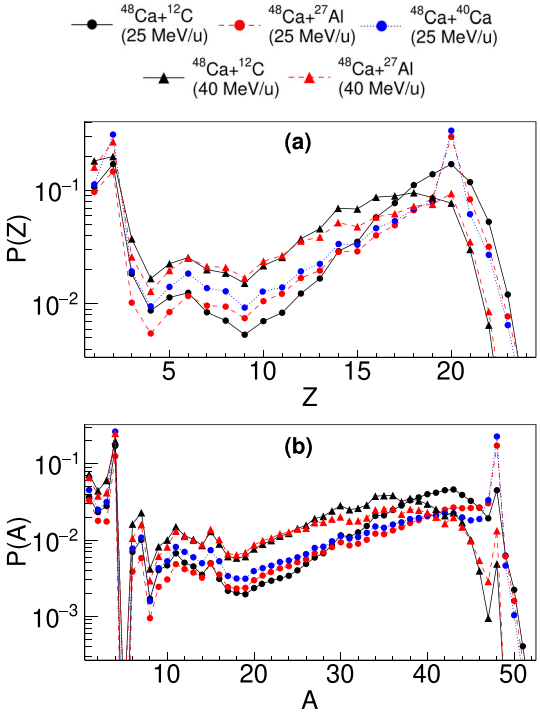

Fig. 3 Probability distribution of (**a**) fragment charge (Z) and (**b**) fragment mass (A) for all fragments detected in the FAZIA-PRE experiment. The distributions are normalized to their events. Statistical uncertainties are smaller than the data symbols

increasing bombarding energy, the ^{27}Al case also changes: the quasi-elastic peak is reduced due to the lower grazing angle and the QP sources are more spread in the phase-space due to larger excitation (see the different shapes of A in the range 30–40 amu at the two energies). We also note, as expected, the abundant production of $Z = 1, 2$ particles. The gap in the A distribution at $A = 5$ is related to the absence of $A = 5$ bound nuclei. This is because of the most unstable and shortest-lived isotope of Helium, ^{5}He, with a half-life of $602(22) \times 10^{-24}$ s [55]. Also, the drop in the mass probability at $A = 8$ is due to the breakage of ^{8}Be into two ^{4}He [56].

Systematic uncertainties in particle identification come from miss-identification of masses and are generally small (± 1 mass number). These miss-identifications are usually present in the valley of the PID peaks [8,9] which have very little contribution to the overall yield. However, we have verified that the results do not change much upon reasonable changes in the assignment of Z and A values. Uncertainties in the energy measurement of particles comes from the detector calibration. The FAZIA collaboration has developed and improved the detection and calibration systems for so many years in such a way that the errors from energy calibration remain around $\sim$1% on the kinetic energies of all particles. Moreover, as far as the statistical uncertainties are concerned, the abundant collected statistics allows us to quote small errors on the presented results that are often less than the chosen size of the symbol in the figures.

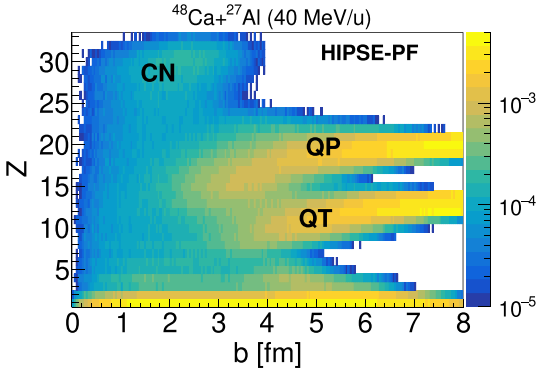

Fig. 4 Fragment charge (Z) vs impact parameter (b) for primary fragments (HIPSE-PF) for ^{48}Ca+^{27}Al (40 MeV/u). The correlation shows the full range of b up to the grazing value

We now have an overall idea of the range of fragments detected in the FAZIA-PRE experiment. In order to extract more specific information from these fragments, we have used the HIPSE event generator to introduce selection rules to be applied to the data.

3 HIPSE simulations

The Heavy-Ion Phase Space Exploration (HIPSE) event generator is a semi-phenomenological model, i.e., consisting of both microscopic and macroscopic modelling approaches, which can simulate intermediate energy nuclear reactions at all impact parameters (b). It can also reproduce some kind of fast (pre-equilibrium) emissions and has demonstrated to be a relatively fast and reliable reaction simulator from light to heavy systems [57], giving, in particular, a good description of QP features for most peripheral collisions [58]. This makes HIPSE one of the most suitable models for us to simulate the data with respect to the FAZIA-PRE experiment and extract the quasi-projectile fragments.

Just to give an idea of the events produced by HIPSE simulations, the output for ^{48}Ca+^{27}Al (40 MeV/u) system is presented in this section. For each reaction system, a total of 1 million events were simulated sampled from a triangular distribution of the full b range (0 to the corresponding b grazing). The primary fragments (HIPSE-PF) Z vs b correlation can be seen in Fig. 4. It is visible that how the various emission sources (marked in the figure) appear with respect to the impact parameter. In particular, they are the excited QP and QT and fusion like fragments (CN). The formation of QT and QP is clearly observed from peripheral to semi-central collisions. The CN yield is increasing with centrality. The excitation energy per nucleon (E^*) gained by the primary fragments is shown in Fig. 5a in correlation with the fragment charge (Z). A detailed structure of E^* can be observed by splitting these fragments according to the emission sources

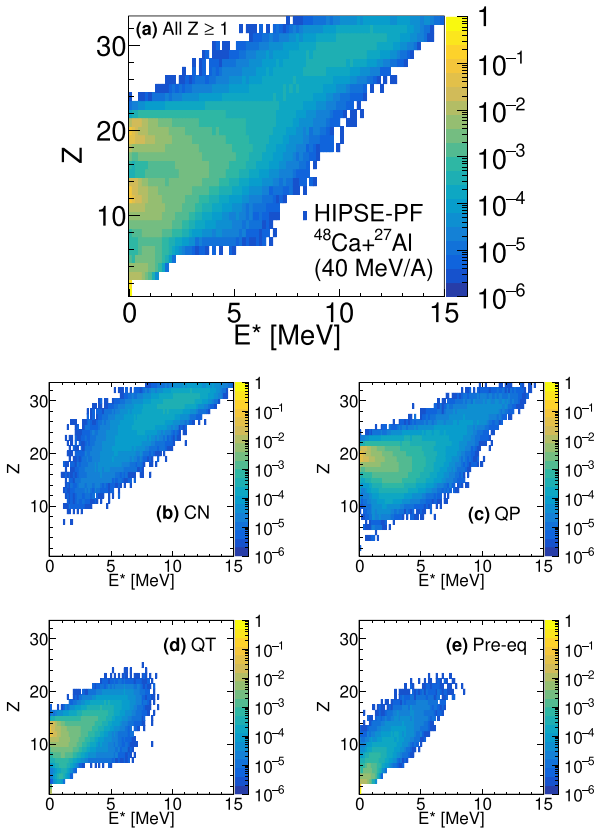

Fig. 5 **a** Primary fragment (HIPSE-PF) charge (Z) vs excitation energy (E^*) distribution obtained in reaction ^{48}Ca+^{27}Al (40 MeV/u) system. **b–e** Similar to (**a**) but split into contributions of various emission sources, namely, fusion-like (CN), quasi-projectile (QP), quasi-target (QT) and pre-equilibrium emissions ($Pre-Eq$), respectively. The z-axis for (**b**)–(**e**) is same as (**a**)

as labelled in the model output for each event (Fig. 5b–e). The QP and QT populate wide regions in $Z - E^*$ plot, corresponding to the impact parameter variation from the grazing collisions (intense yellow regions at low E^*) to the central collisions. CN source corresponds to the largest and most excited fragments (note the E^* values even higher than the typical nuclear binding energies). The pre-equilibrium ($Pre-eq$) fragments are present throughout the b range and are relatively light with excitation energy mostly below 5 MeV.

These primary fragment data are passed through de-excitation codes like SIMON [59] or GEMINI++ [60] to get the secondary fragments. In this work, we will focus only on the final products from GEMINI++ de-excitation code. Figure 6a shows the Z vs $v_{\parallel}$ correlation of full 4π distributed HIPSE-GEMINI++ fragments boosted to the laboratory frame. The QT and QP are marked and clearly visible in the figure. The QT region corresponds to $v_{\parallel} \sim 0$ as the target is at rest in the lab and emissions from its phase space are slow. On the other hand, the QP region lies near

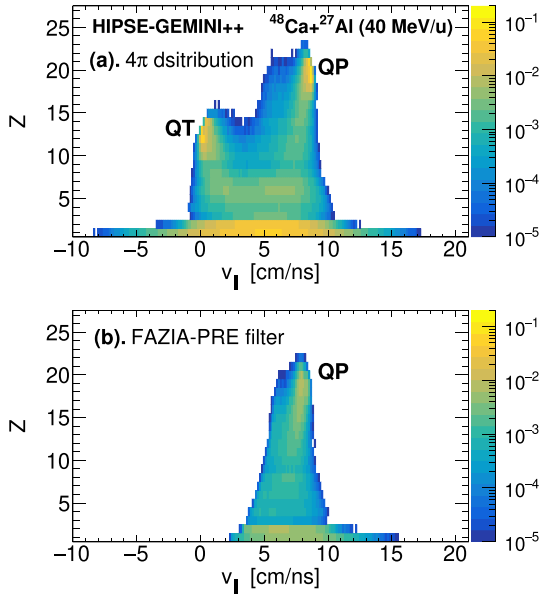

Fig. 6 Fragment charge (Z) vs longitudinal velocity ($v_\parallel$) distribution for ^{48}Ca+^{27}Al (40 MeV/u) system. (**a**) Full 4π HIPSE-GEMINI++ distribution. (**b**) HIPSE-GEMINI++ simulation after FAZIA-PRE experimental filter. Both data are normalised to their number of events

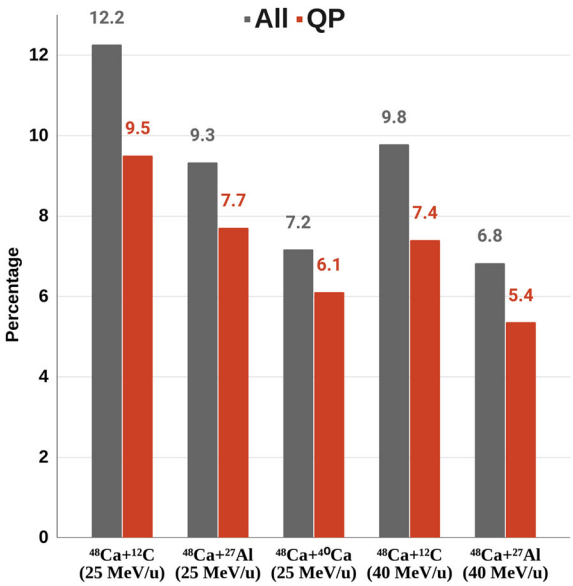

Fig. 7 Model data: percentages of detected fragments in the FAZIA-PRE setup, calculated from filtered HIPSE-GEMINI++ simulations. The blue bars correspond to all the charged fragments detected that are coming from various processes and emission sources. The red bars correspond to the detected fragments labelled in HIPSE to be generated from the QP region

the beam velocity, which, for this system, is $\sim$ 8.5 cm/ns. Notwithstanding the good coverage for QP phase-space, the efficiency of the experimental setup is limited and, cuts and distortions can be introduced by the detection system. Therefore, the full 4π HIPSE-GEMINI++ data are filtered according to the experimental constraints, i.e. detector geometry, energy thresholds, detector resolution, etc. applied through the KaliVeda frameworks [61]. The output of the filtered simulation is shown in Fig. 6b. Comparing the data before and after applying the experimental filter, it can be observed that the filtered data conserves the QP region well, while removing the QT phase space. We point out the strict similarity of Fig. 6b with the experimental correlation of the corresponding reaction in Fig. 2e.

According to the calculations from filtered HIPSE-GEMINI++ simulations, the percentage of the detected charged fragments out of the whole 4π distribution for the FAZIA-PRE setup is given in Fig. 7 showing the detection efficiency for all fragments (All, blue bars) and QP fragments (red bars). The calculated efficiency range is 7–12%. However, as expected, according to the model, most of the "detected" ejecta (above 70% overall) are QP fragments; this reinforces the hypothesis that the measured events are mostly compatible with QP and related emission as we will more precisely discuss in the next section.

4 Data comparison and results

In this section, we will introduce selections in the experimental data to extract the QP fragments and then compare the experimental results with the filtered HIPSE-GEMINI++ simulations.

We want to restrict to the events where the largest QP fragments do not undergo further break-up or fragmentation. Hence, after the secondary decays, they must be detected as QP remnants. To exclude the lighter fragments and QP break-up channel, we put two conditions. Firstly, we choose only those events in which a single fragment was detected. So, we put the condition on the total charged particle multiplicity to be 1. Secondly, we put a cut on the fragment charge to be $Z > 10$, which is greater than half of the projectile Z. This selection strongly reduces the probability to have two smaller products from complete projectile split processes and removes the smaller fragment from each break-up pair. According to the model, the remaining spurious events (not-QP) with fake QP attribution are well less than 20% for all investigated reactions. Henceforth, this selection will be referred to as the QP-*cut*.

This QP-*cut* applied to the filtered HIPSE simulations is further applied to the experimental data as well. The direct comparison of HIPSE and the experimental data (EXP) after the QP-*cut* is shown in Fig. 8. The figure shows the comparison for basic reaction observables, Z (Fig. 8a–e) and A (Fig. 8f–j). Each row represents a reaction system. From the Z distributions, one can infer that HIPSE well reproduces the experimental data. On the other hand, from the A distributions, there is good agreement between the HIPSE

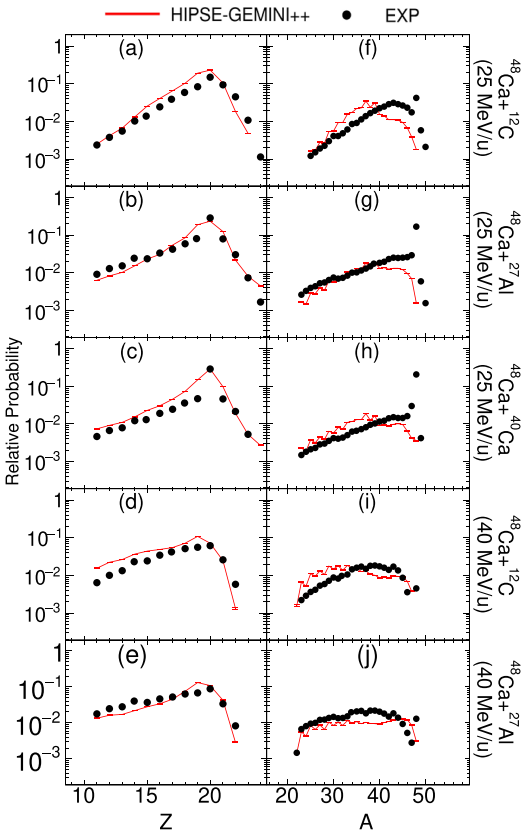

Fig. 8 Comparison of the filtered HIPSE-GEMINI++ data with the FAZIA-PRE experimental data (EXP) after applying the *QP-cut*. (**a**)–(**e**) Charge (Z) distributions ; (**f**)–(**j**) mass (A) distributions. Each row represents a reaction system

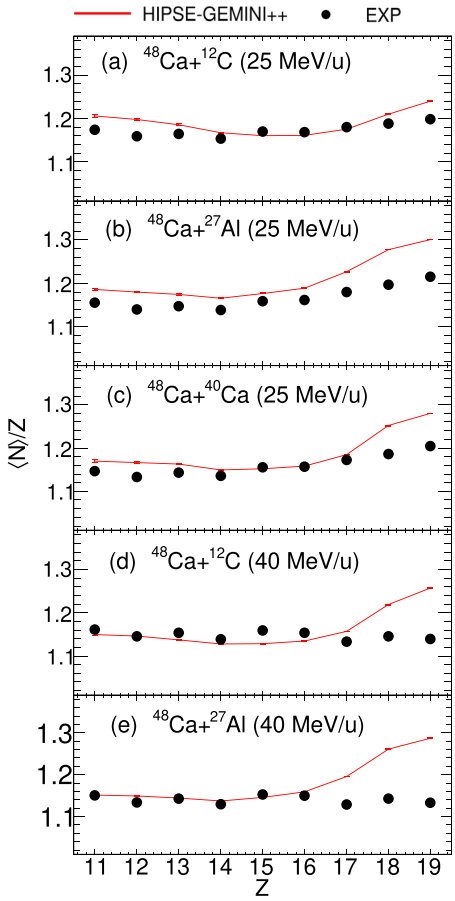

Fig. 9 The fragment $\langle N\rangle/Z$ vs Z correlation for all FAZIA-PRE systems to compare HIPSE-GEMINI++ and experimental data (EXP) after applying the *QP-cut*

and experimental data except for the region of the heaviest masses in particular at the lower beam energy. Indeed for these reactions the experimental data contain some residual contribution (peak at $A = 48$) from very peripheral (almost elastic scattering) events. The observed mass distribution differences between model and data can be explained considering that the projectile is neutron rich. So the statistical evaporation of neutrons is favored during the decay. On the other hand, the model does not include the elastic scattering cross section and perhaps the modelling of the very peripheral reactions is not well performed. At 40 MeV/u the model and the experimental mass distributions are closer because the original yield and acceptance make the quasi-elastic channel contribution in the experimental data to be lower. Moreover, the Z distributions are less modified, so the agreement between model and data remains at a better level than for the nuclear masses.

With this caveat in mind and considering the observed overall reasonable agreement between HIPSE and experimental data for basic reaction observables, we also checked the consistency for a more characteristic observable, i.e., the mean fragment isospin ($\langle N\rangle/Z$). The FAZIA detector, with its excellent isotopic resolution allows for refined fragment N/Z studies. Concerning this observable, it is stated in the original HIPSE article [50] that the calculations give the final charge to mass ratio of fragments created during the reaction and thus it could be chosen to explore the N/Z effects in nuclear collisions in the Fermi-energy range. The fragment $\langle N\rangle/Z$ vs Z is shown in Fig. 9a–e for all FAZIA-PRE systems. The *QP-cut* has been applied to the data presented in the figure. It can be observed from this comparison that HIPSE satisfactorily reproduces the shape of the mean fragment isospin up to $Z \sim 16$. Taking into account the previous comment on the limitation of the model towards the most peripheral collisions, the agreement up to $Z \sim 16$ is reasonable. Indeed it suggests that the model describes the N/Z of fragments coming from rather damped reactions fairly well, having final detected charges quite below the projectile value (here $Z = 15$–16).

Since the entrance channel properties in terms of reacting nuclei are rather well described by HIPSE, we now move to study the variation of beam energy, thanks to the two sets of measured data at 25 and 40 MeV/u. We can use the fragment

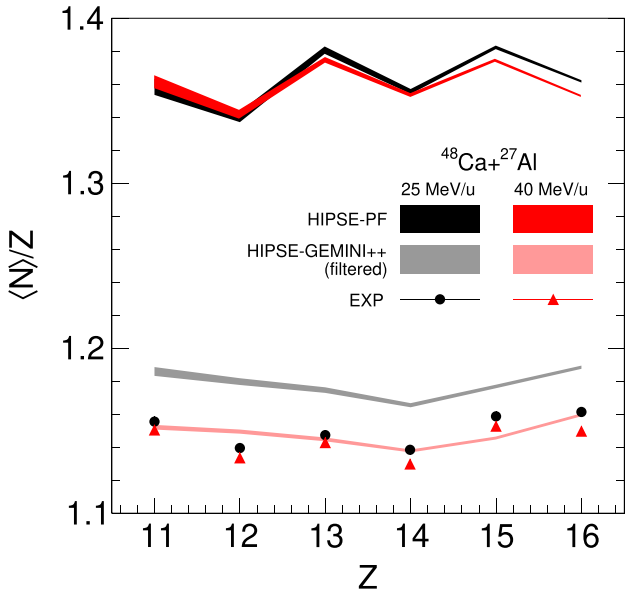

Fig. 10 $\langle N\rangle/Z$ vs Z for ^{48}Ca + ^{27}Al system after QP-*cut* to observe the effect of changing beam energy. Black band for 25 MeV/u and red band for 40 MeV/u for HIPSE-PF (primary fragments); grey and pink bands for filtered HIPSE-GEMINI++ data and experimental data in black circles for 25 MeV/u and red triangles for 40 MeV/u systems (same data from Fig. 9)

N/Z to observe the entrance channel effects of beam energy. For this, ^{40}Ca system is not useful because it is only present for 25 MeV/u. Moreover, as we focus on the QP fragment, the ^{12}C systems will also not be considered. A detailed study of the ^{12}C systems from this experiment is given in Ref. [10].

In Ref. [52], it is clearly stated that the additional available energy is mainly removed by the pre-equilibrium emissions from the system. The pre-equilibrium neutron multiplicity keeps on increasing with the beam energy. On the other hand, the rate of thermalisation saturates softly after 20 MeV/u. So, in our case, where the beam energies are 25 and 40 MeV/u, we might expect that the pre-equilibrium emissions are playing a role. This means that if we observe the QP region in the primary fragments, the fragment N/Z should decrease with increasing beam energy. The Fig. 10 shows the $\langle N\rangle/Z$ vs Z comparison w.r.t. beam energy for HIPSE-PF, filtered HIPSE-GEMINI++ and the experimental data for ^{48}Ca+^{27}Al system. Let's start with the model predictions. It can be seen that the $\langle N\rangle/Z$ is, in general, slightly lower for 40 MeV/u system (especially for the largest remnants). The secondary decays, as expected, then further and strongly reduce the overall fragment $\langle N\rangle/Z$ but still are able to preserve the original primary hierarchy even when the FAZIA-PRE experimental constraints are introduced. Moving to the experimental results (drawn with symbols), we see that the data at 40 MeV/u are systematically below those at 25 MeV/u. The effect is smaller than predicted by HIPSE.

We are aware that there are multiple effects under consideration that alter the fragment $\langle N\rangle/Z$; therefore it is a difficult task for the models, and also for HIPSE, to accurately describe all those effects. From this respect we can observe that HIPSE is qualitatively successful in predicting the observed charge and mass distributions, for pre-equilibrium and post thermalization phases. The discrepancies for the lower presented energy are below 0.5 neutron and do not change the overall outcome. The trend seen in experimental data is preserved. The intuitive idea about increasing preferential neutron pre-equilibrium emissions with beam energy is not excluded but cannot be confirmed, as the large differences in $\langle N\rangle/Z$ result from the de-excitation of the hot QP remnants coming from neutron-rich induced dissipative collisions. However, Fig. 10 suggests that some effect with increasing beam energy occurs at least for the heaviest fragments (primary fragments close to the Z of projectile). In the experimental data, although strongly quenched by evaporation, a tension towards a difference from 25 to 40 MeV/u for the same heavy fragments, persists.

5 Summary and conclusion

This work focused on the analysis of the data from the FAZIA-PRE experiment, performed using 6 FAZIA blocks at LNS-INFN (Italy). The measured reaction systems were ^{48}Ca + ^{12}C, ^{27}Al (25, 40 MeV/u) and ^{48}Ca + ^{40}Ca (25 MeV/u). The full range of charge and mass of the detected fragments was identified in the experiment. The data for all systems showed high intensity of fragments similar to the projectile as well as around the beam velocities (quasi-projectile fragments).

We used the HIPSE event generator to produce the simulated events like in the FAZIA-PRE reaction systems. The HIPSE secondary fragments were obtained in a full 4π distribution using the GEMINI++ de-excitation code. This HIPSE-GEMINI++ data were filtered according to the FAZIA-PRE experimental constraints and it was confirmed that the detected fragments are mostly originating from quasi-projectile fragments. Constraints were put following the indications from HIPSE to obtain the single largest quasi-projectile fragment from each collision event. The data from HIPSE and the experiment were then compared after applying these constraints. It was seen that HIPSE gives a good overall reproduction of the experimental data with respect to inclusive fragment observables. Furthermore, HIPSE is able to produce the general trend of the fragment ⟨N⟩/Z with respect to the experimental data, excluding the QP charges associated to very peripheral collisions, not well described by the model. The measured average N/Z values of the QP remnants are lower at 40 than at 25 MeV/u beam energy. Although in a qualitative way, the comparison with the model

predictions cannot exclude a role of pre-equilibrium neutron emissions that increase with increasing beam energy. Indeed, in combination with the particle evaporation that significantly affects the N/Z of remnants, the slight increasing free neutron fast emissions from the neutron rich transient sources before evaporation can also have a role in determining the measured isotopic distributions. This intricate subject can be further explored by comparing the data with other intermediate energy nuclear reaction models like the antisymmetrized molecular dynamics (AMD) model [62], stochastic mean field (SMF) model [63], etc.

From the results obtained in this work, we can conclude that the HIPSE event generator has proved also in this case to be a fine tool to generate the fragments in nuclear reactions at intermediate energy range and to satisfactorily describe the basic reaction dynamics.

Acknowledgements We would like to thank the accelerator staff of INFN-LNS laboratories for having provided good-quality beams and support during the experiment. This work was partially supported by the POLITA grant: project HARMONIA No. UMO-2014/14/M/ST2/00738 (COPIN-INFN Collaboration) and the Jagiellonian University DS research grant (K/DSC/005311/2018).

Data Availability Statement Data will be made available on reasonable request. [Authors' comment: The datasets generated during and/or analysed during the current study are available from the corresponding author on reasonable request.]

Code Availability Statement Code/software will be made available on reasonable request. [Authors' comment: The code/software generated during and/or analysed during the current study is available from the corresponding author on reasonable request.]

References

1. I. Iori et al., Nucl. Instrum. Methods Phys. Res. Sect. A Acceler. Spectrom. Detect. Assoc. Equip. **325**(3), 458 (1993). https://doi.org/10.1016/0168-9002(93)90391-T
2. F. Gramegna, et al., in *IEEE Symposium Conference Record Nuclear Science 2004*, vol. 2 (2004), pp. 1132–1136. https://doi.org/10.1109/NSSMIC.2004.1462402
3. S. Aiello et al., Nucl. Phys. A **583**, 461 (1995). https://doi.org/10.1016/0375-9474(94)00705
4. J. Łukasik et al., Nucl. Instrum. Methods Phys. Res. Sect. A Acceler. Spectrom. Detect. Assoc. Equip. **709**, 120 (2013). https://doi.org/10.1016/j.nima.2013.01.029
5. NIMROD, Multipurpose charged particle array at Texas A&M University. https://cyclotron.tamu.edu/nimrod/
6. N. Madhavan et al., Pramana J. Phys. **75**(2), 317 (2010). https://doi.org/10.1007/s12043-010-0119-3
7. R. Bougault et al., Eur. Phys. J. A **50**(2), 47 (2014). https://doi.org/10.1140/epja/i2014-14047-4
8. D. Gruyer et al., Nucl. Instrum. Methods Phys. Res. Sect. A Acceler. Spectrom. Detect. Assoc. Equip. **847**, 142 (2017). https://doi.org/10.1016/j.nima.2016.11.062
9. G. Pastore et al., Nucl. Instrum. Methods Phys. Res. Sect. A Acceler. Spectrom. Detect. Assoc. Equip. **860**, 42 (2017). https://doi.org/10.1016/j.nima.2017.01.048
10. S. Piantelli et al., Phys. Rev. C **107**, 044607 (2023). https://doi.org/10.1103/PhysRevC.107.044607
11. S. Barlini et al., Phys. Rev. C **87**, 054607 (2013). https://doi.org/10.1103/PhysRevC.87.054607
12. A. Camaiani et al., Phys. Rev. C **102**, 044607 (2020). https://doi.org/10.1103/PhysRevC.102.044607
13. S. Piantelli et al., Phys. Rev. C **101**, 034613 (2020). https://doi.org/10.1103/PhysRevC.101.034613
14. S. Piantelli et al., Phys. Rev. C **103**, 014603 (2021). https://doi.org/10.1103/PhysRevC.103.014603
15. A. Camaiani et al., Phys. Rev. C **103**, 014605 (2021). https://doi.org/10.1103/PhysRevC.103.014605
16. C. Ciampi et al., Phys. Rev. C **106**, 024603 (2022). https://doi.org/10.1103/PhysRevC.106.024603
17. A. Pagano et al., Eur. Phys. J. A **56**(4), 102 (2020). https://doi.org/10.1140/epja/s10050-020-00105-z
18. P. Chomaz, F. Gulminelli, W. Trautmann, S. Yennello, Dynamics and thermodynamics with nuclear degrees of freedom. Eur. Phys. J. A **30**(thematic issue 1), 1–251 (2006)
19. E. Galichet et al., Phys. Rev. C **79**, 064614 (2009). https://doi.org/10.1103/PhysRevC.79.064614
20. D.V. Shetty, S.J. Yennello, G.A. Souliotis, Phys. Rev. C **76**, 024606 (2007). https://doi.org/10.1103/PhysRevC.76.024606
21. B.A. Li, L.W. Chen, C.M. Ko, Phys. Rep. **464**(4), 113 (2008). https://doi.org/10.1016/j.physrep.2008.04.005
22. M.D. Toro, V. Baran, M. Colonna, V. Greco, J. Phys. G Nucl. Part. Phys. **37**(8), 083101 (2010). https://doi.org/10.1088/0954-3899/37/8/083101
23. F. Rami et al., Phys. Rev. Lett. **84**, 1120 (2000). https://doi.org/10.1103/PhysRevLett.84.1120
24. I. Lombardo et al., Phys. Rev. C **82**, 014608 (2010). https://doi.org/10.1103/PhysRevC.82.014608
25. E. Geraci et al., Nucl. Phys. A **732**, 173 (2004). https://doi.org/10.1016/j.nuclphysa.2003.11.055
26. G. Souliotis, M. Veselsky, D. Shetty, S. Yennello, Phys. Lett. B **588**(1), 35 (2004). https://doi.org/10.1016/j.physletb.2004.03.027
27. M.B. Tsang et al., Phys. Rev. Lett. **92**, 062701 (2004). https://doi.org/10.1103/PhysRevLett.92.062701
28. M.B. Tsang et al., Phys. Rev. Lett. **102**, 122701 (2009). https://doi.org/10.1103/PhysRevLett.102.122701
29. Z.Y. Sun et al., Phys. Rev. C **82**, 051603 (2010). https://doi.org/10.1103/PhysRevC.82.051603
30. M. Veselsky et al., Phys. Rev. C **62**, 041605 (2000). https://doi.org/10.1103/PhysRevC.62.041605
31. E. De Filippo et al., Phys. Rev. C **86**, 014610 (2012). https://doi.org/10.1103/PhysRevC.86.014610
32. V. Baran, M. Colonna, V. Greco, M. Di Toro, Phys. Rep. **410**(5), 335 (2005). https://doi.org/10.1016/j.physrep.2004.12.004
33. L.W. Chen, C.M. Ko, B.A. Li, Phys. Rev. Lett. **94**, 032701 (2005). https://doi.org/10.1103/PhysRevLett.94.032701
34. T.X. Liu et al., Phys. Rev. C **76**, 034603 (2007). https://doi.org/10.1103/PhysRevC.76.034603
35. B.A. Li, W.U. Schröder, *Isospin Physics in Heavy-Ion Collisions at Intermediate Energies* (Nova Science, New York, 2001)

36. G.A. Souliotis et al., Phys. Rev. C **68**, 024605 (2003). https://doi.org/10.1103/PhysRevC.68.024605
37. M. Colonna, J. Rizzo, P. Chomaz, M. Di Toro, Nucl. Phys. A **805**(1), 454c (2008). https://doi.org/10.1016/j.nuclphysa.2008.02.266.INPC2007
38. L.W. Chen, B.J. Cai, C.M. Ko, B.A. Li, C. Shen, J. Xu, Phys. Rev. C **80**, 014322 (2009). https://doi.org/10.1103/PhysRevC.80.014322
39. E. Galichet, M. Colonna, B. Borderie, M.F. Rivet, Phys. Rev. C **79**, 064615 (2009). https://doi.org/10.1103/PhysRevC.79.064615
40. Q. Fable et al., (2023). https://doi.org/10.48550/arXiv.2312.01763. arXiv:2312.01763 [nucl-ex]
41. R.T. de Souza, W.U. Schröder, J.R. Huizenga, R. Planeta, K. Kwiatkowski, V.E. Viola, H. Breuer, Phys. Rev. C **37**, 1783 (1988). https://doi.org/10.1103/PhysRevC.37.1783
42. R. Planeta et al., Phys. Rev. C **38**, 195 (1988). https://doi.org/10.1103/PhysRevC.38.195
43. D. Thériault et al., Phys. Rev. C **74**, 051602 (2006). https://doi.org/10.1103/PhysRevC.74.051602
44. A.B. McIntosh et al., Phys. Rev. C **81**, 034603 (2010). https://doi.org/10.1103/PhysRevC.81.034603
45. S. Hudan et al., Phys. Rev. C **86**, 021603 (2012). https://doi.org/10.1103/PhysRevC.86.021603
46. Q. Fable et al., Phys. Rev. C **106**, 024605 (2022). https://doi.org/10.1103/PhysRevC.106.024605
47. C. Ciampi et al., J. Phys. Conf. Ser. **2586**(1), 012039 (2023). https://doi.org/10.1088/1742-6596/2586/1/012039
48. Q. Fable et al., Phys. Rev. C **107**, 014604 (2023). https://doi.org/10.1103/PhysRevC.107.014604
49. C. Ciampi et al., Phys. Rev. C **108**, 054611 (2023). https://doi.org/10.1103/PhysRevC.108.054611
50. D. Lacroix, A. Van Lauwe, D. Durand, Phys. Rev. C **69**, 054604 (2004). https://doi.org/10.1103/PhysRevC.69.054604
51. D. Lacroix, A. Van Lauwe, D.D. Durand, in *International Workshop on Multifragmentation and Related Topics (IWM2003)*. ed. by L. Wieleczko (Infn Catania, CAEN, France, 2003), pp.58–61
52. L. Lassen, P. von Neumann-Cosel, A. Oberstedt, G. Schrieder, Phys. Rev. C **55**, 1900 (1997). https://doi.org/10.1103/PhysRevC.55.1900
53. S. Carboni et al., Nucl. Instrum. Methods Phys. Res. Sect. A Acceler. Spectrom. Detect. Assoc. Equip. **664**(1), 251 (2012). https://doi.org/10.1016/j.nima.2011.10.061
54. B. Braunn et al., Nucl. Instrum. Methods Phys. Res. Sect. B **269**(22), 2676 (2011). https://doi.org/10.1016/j.nimb.2011.08.010
55. F. Kondev, M. Wang, W. Huang, S. Naimi, G. Audi, Chin. Phys. C **45**(3), 030001 (2021). https://doi.org/10.1088/1674-1137/abddae
56. H. Schatz, K. Blaum, Europhys. News **37**(5), 16 (2006). https://doi.org/10.1051/epn:2006502
57. C. Frosin et al., Phys. Rev. C **107**, 044614 (2023). https://doi.org/10.1103/PhysRevC.107.044614
58. D. Lacroix, Quantum nuclear many-body dynamics and related aspects. Research report, CNRS. Mémoire de HDR soutenu le 16 décembre 2010, Université de Caen-Basse Normandie (2011)
59. D. Durand, Nucl. Phys. A **541**(2), 266 (1992). https://doi.org/10.1016/0375-9474(92)90097-4
60. R.J. Charity, Joint ICTP-IAEA advanced workshop on model codes for spallation reactions, Trieste, IAEA, Report INDC(NDC)-0530 (2008), p. 139
61. KaliVeda Toolkit, https://kaliveda.in2p3.fr/
62. Y. Kanada-En'yo, M. Kimura, A. Ono, Progr. Theor. Exp. Phys. **2012**(1), 01A202 (2012). https://doi.org/10.1093/ptep/pts001
63. M. Colonna et al., Nucl. Phys. A **642**(3), 449 (1998). https://doi.org/10.1016/S0375-9474(98)00542-9